


Behavior of Steel–Lightweight Self Compacting Concrete Composite Beams with Various Degrees of Shear Interaction

Bayadir Abed Hadi ¹, Samoel Mahdi Saleh ^{1*} 

¹ College of Engineering, University of Basrah, Basrah 61004, Iraq.

Received 14 July 2023; Revised 21 October 2023; Accepted 26 October 2023; Published 01 November 2023

Abstract

This study investigated the use of lightweight self-compacting concrete (LWSCC), which represents a trend in producing high-performance concrete, as slabs in steel-concrete composite beams with headed studs as shear connectors. Three push-out test specimens were fabricated and tested to assess the shear strength and behavior of M16-headed stud connectors embedded in LWSCC. Based on the push-out test results, six steel-LWSCC composite beams were manufactured and tested as simply supported composite beams. In addition, a steel-normal weight self-compacting concrete (NWSCC) composite beam specimen with full shear interaction was manufactured and tested for comparison. The main variables taken into account in this study were the degree of shear interaction and regions of bending moment (sagging or hogging). It was observed that the increase in degree of shear interaction from 50 to 100% improved the ultimate carrying capacity, the service load, and the stiffness of the tested steel-LWSCC beam specimens by a ratio reached to 96, 95, and 122%, respectively, when subjected to sagging bending moments and by a ratio reached to 57, 59, and 134%, respectively, when subjected to hogging bending moments. In addition, it was noted that the deflection and the end slip values for steel-LWSCC specimens under a sagging bending moment are smaller than those under a hogging bending moment, which have the same degree of shear interaction and at the same load level. Moreover, the experimental results show that the ultimate carrying capacity, service load, and stiffness values for the steel-NWSCC composite beam were higher than those for the steel-LWSCC beam specimens that have the same properties, while the ultimate deflection and end slip were smaller.

Keywords: Composite Beam; Shear Connection; Lightweight Concrete; Self-Compacting Concrete; Pushout Test; Sagging Bending Moment; Hogging Bending Moment.

1. Introduction

Nowadays, it is common in building and bridge construction to use a concrete slab supported by steel beams connected together to behave as one unit, which is called composite beams. As compared to steel or reinforced concrete beams, conventional steel-concrete composite beams exhibit better structural properties in terms of stiffness and strength. The improvement in the structural properties of such composite beams primarily depends on the type and efficiency of the shear connections between the steel beam and concrete slab, as well as the structural performance of the two components [1–4]. Although many researchers have investigated the structural behavior of steel-concrete composites considering the effect of different states of loading along with the effect of different material parameters and different shear interaction methods [5–13], the study of the behavior of composite beams made from new types of concrete, like self-compacting concrete, sometimes called green concrete, is still limited.

It is clearly known that the weight reduction with the use of lightweight concrete for composite beams can improve the construction cost by increasing the beam spans or reducing the sizes of steel sections to produce lighter structures and then shallower and smaller foundations. Moreover, in spite of the fact that self-compacting concrete has been

* Corresponding author: samoel.saleh@uobasrah.edu.iq



<http://dx.doi.org/10.28991/CEJ-2023-09-11-04>



© 2023 by the authors. Licensee C.E.J, Tehran, Iran. This article is an open access article distributed under the terms and conditions of the Creative Commons Attribution (CC-BY) license (<http://creativecommons.org/licenses/by/4.0/>).

available for many years, its use in building construction has recently increased due to its benefits in terms of cost reduction and environmental efficiency that come from its ability to spread and fill the structure's formwork even with congested reinforcement without any mechanical vibration. Therefore, lightweight self-compacting concrete (LWSCC) can be a very attractive material in the design and construction of composite beams for different types of structures.

The different properties of self-compacting concrete (SCC) have been investigated in several studies over the past few years. In some of these studies, classical engineering testing procedures were employed, while others used pathless techniques, such as non-destructive testing procedures or artificial neural network numerical models, to predict the quality and mechanical properties of such a type of concrete [14–18]. However, intensive research has been conducted on the characterization and production of LWSCC in order to provide more information and design data [19–22]. LWSCC is essentially produced by using lightweight aggregates, which may be divided into two kinds: natural and artificial aggregates [23]. A major objective of using self-compacting concrete in LWSCC is to reduce the total volume of cementitious materials to the maximum extent possible [24]. Moreover, the use of some cementation materials, such as fly ash and silica fume, in the production of LWSCC may improve the interfaces between the cement matrix and the lightweight aggregate, which represents a weak point in normal vibrated lightweight concrete [25].

In the present work, the structural behavior of steel-LWSCC composite beams has been investigated. For the adopted mixes of LWSCC, a light expanded clay aggregate (Leca) was used as coarse aggregate. A LWSCC made from this type of lightweight aggregate may have highly workable and durable properties compared with the use of other lightweight aggregates [26–28]. Six beam specimens were fabricated with three different degrees of shear interaction to examine the effect of loading type (sagging or hogging bending moment) and degree of shear interaction on the behavior of such composite beams. The headed stud shear connections were selected to connect the steel beams with LWSCC slabs, which represent the most common type of shear connectors. The efficiency of the headed stud shear connectors was evaluated by testing three push-out test specimens. In addition, a composite beam specimen made with normal-weight self-compacting concrete was fabricated for comparison.

2. Materials and Methods

2.1. Test Specimens

2.1.1. Push-out Test Specimens

Three repeated pushout test specimens were fabricated in order to evaluate the shear capacity and load-slip relationship of the adopted stud shear connectors embedded in LWSCC. Figure 1 shows the details of the push-out test specimens, where two (500 × 500 × 150 mm) LWSCC slabs were attached to a 500 mm length of HE200B steel column by using two 90 mm long M16-headed studs in each slab. Each LWSCC concrete slab was reinforced with two layers of 10 mm steel reinforcement bars arranged horizontally and longitudinally.

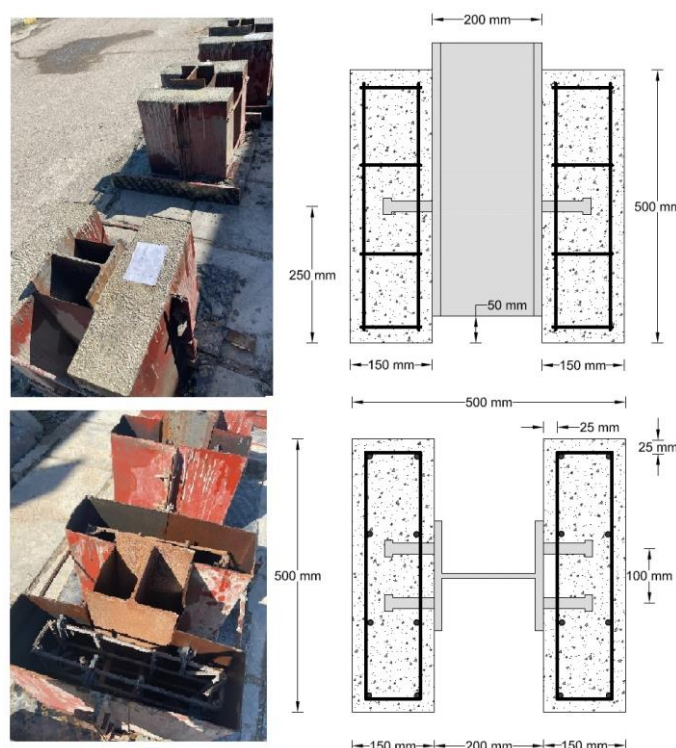


Figure 1. Details of pushout test specimens

2.1.2. Composite Beam Specimens

A total of six steel-LWSCC composite beams were fabricated to be tested under a three-point loading effect. Each composite beam has an IPE140 European steel beam attached to the LWSCC slab with a width and thickness equal to 400 mm and 120 mm, respectively. M16-headed studs were used as shear connectors, whereas the concrete slabs were provided by two layers of 10 mm steel reinforcement bars with a spacing of about 100 mm in each direction, as shown in Figure 2. Three different degrees of shear interaction were used in order to evaluate their effect on the behavior of such composite beams under the action of sagging and hogging bending moments. Another steel-normal-weight self-compacting concrete composite beam was designed with the same details as other beam specimens for comparison. The details of the composite beam specimens are listed in Table 1.

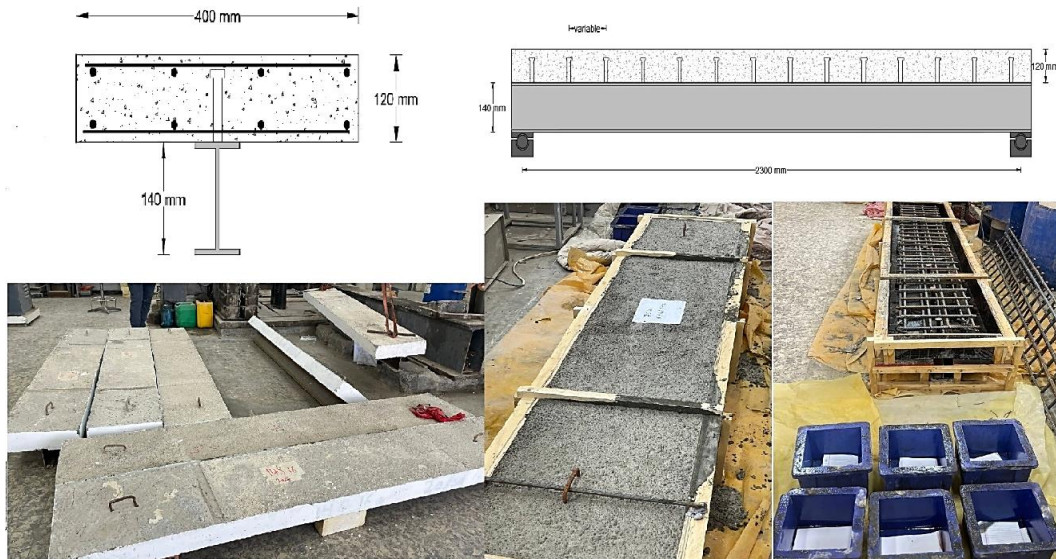


Figure 2. Details of composite beam specimens

Table 1. Details of composite beam specimens

Specimens' designation	L100(16)S	L075(16)S	L050(16)S	L100(16)H	L075(16)H	L050(16)H	N100(16)S
Span length (mm)	2300	2300	2300	2300	2300	2300	2300
Steel beam section	IPE140	IPE140	IPE140	IPE140	IPE140	IPE140	IPE140
Concrete slab width (mm)	400	400	400	400	400	400	400
Concrete slab thickness (mm)	120	120	120	120	120	120	120
Concrete type	LWSCC	LWSCC	LWSCC	LWSCC	LWSCC	LWSCC	NWSCC
Concrete Cube compressive strength, f_{cu} (MPa)	36.7	36.7	36.7	35.0	35.0	35.0	37.5
Concrete density (kg/m ³)	1810	1810	1810	1792	1792	1792	2365
Stud diameter \times length (mm)	M16 \times 90	M16 \times 90	M16 \times 90	M16 \times 90	M16 \times 90	M16 \times 90	M16 \times 90
Number of studs	14	10	7	14	10	7	14
Longitudinal stud spacing (mm)	170	240	340	170	240	340	170
Degree of interaction (%)	100	75	50	100	75	50	100
Applied bending moment	Sagging	Sagging	Sagging	Hogging	Hogging	Hogging	Sagging

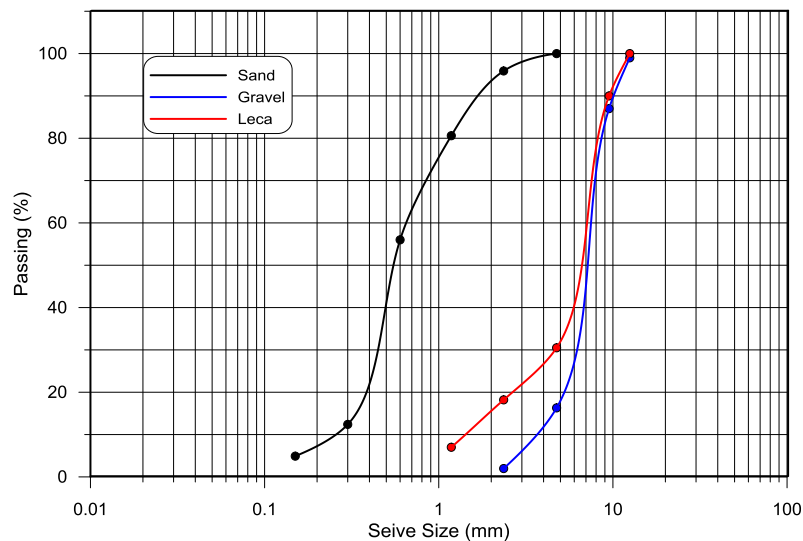
2.2. Materials

To achieve the goals of the present study, a LWSCC mix with a target cube compressive strength of about 30 MPa was developed using light expanded clay aggregate (leca) as a lightweight coarse aggregate in combination with normal density coarse (gravel) and fine (sand) aggregates, cement, limestone powder (LP), superplasticizer (SP), and water. On the other hand, the adopted materials for the NWSCC mix were sand, gravel, cement, limestone powder, and water. The details of the adopted concrete mixes and the properties of fresh concrete, which were evaluated according to EN 206-9: 2010 specifications, are shown in Table 2.

Table 2. Details and properties of adopted concrete mixes

Concrete mix	LWSCC	NWSCC
Water cement ratio	0.44	0.35
Cement (kg/m ³)	450	370
Lightweight coarse aggregate, leca (kg/m ³)	280	----
Normal coarse aggregate, gravel (kg/m ³)	180	720
Fine coarse aggregate, sand (kg/m ³)	800	1100
Limestone powder, LP (kg/m ³)	150	160
Superplasticizer, SP (L/m ³)	6.6	7.4
Slump flow value (mm)	740	750
Blocking ratio	0.99	0.94
Sieve segregation (%)	4.5	8.8

The particle size distributions of the adopted fine and coarse aggregates (leca, gravel, and sand) are shown in Figure 3 with a maximum particle size of about 9.5 and 12.5 mm for leca and gravel, respectively, and about 2.36 mm for sand. Table 3 shows the physical properties of the coarse and fine aggregates, which were evaluated according to BS812-110: 1990 specification.

**Figure 3. Particle size distribution of fine and coarse aggregates****Table 3. Details and properties of adopted concrete mixes**

Material	Gravel	Leca	Sand
Maximum size (mm)	12.5	9.5	2.36
Specific gravity	2.65	1.38	2.67
Absorption (%)	1.34	11.4	1.07
Loose bulk density ((kg/m ³)	1710	1540	790

Six (150×150×150 mm) standard concrete cubes were casted for each concrete batch during the fabrication of pushout and beam specimens in order to evaluate the density and actual compressive strength (f_{cu}) of the specimens' concrete slabs, see Table 1. The mechanical properties of steel beam, steel reinforcement, and headed stud, which were evaluated according to ASTM A370-14, are shown in Table 4.

Table 4. Mechanical characteristics of steel

Steel type	Yield strength, f_y (MPa)	Ultimate strength f_u (MPa)
Reinforcement ($\Phi 10$)	470	620
Steel Beam (IPE140)	290	430
Headed stud (M16)	440	530

The adopted systematic procedure, which previously explained for the experimental work of the present study, can be summarized as shown in Figure 4.

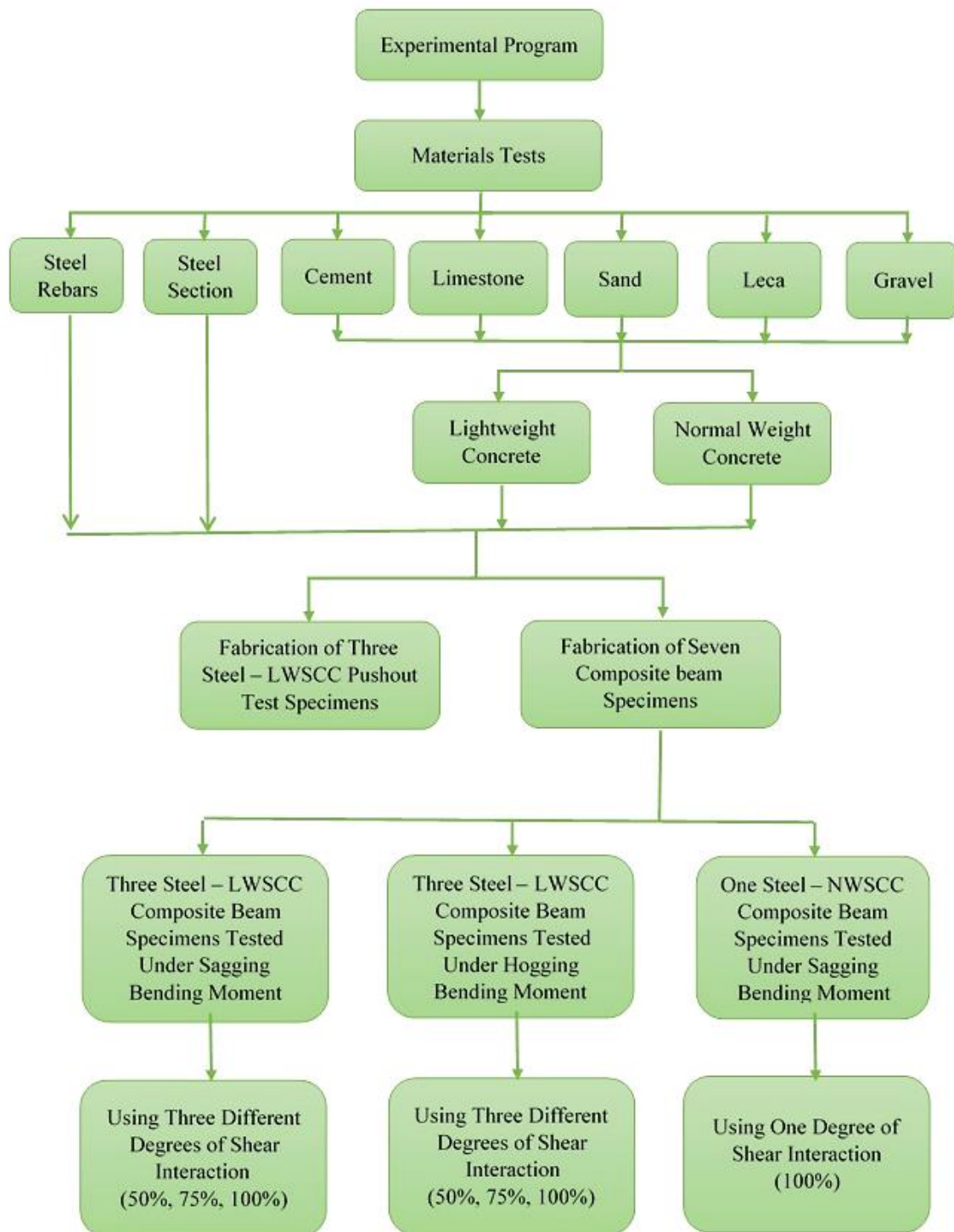


Figure 4. Experimental program's flowchart

2.3. Loading and Test Procedure

Both the pushout and beam test specimens were tested by applying monotonic loading from a universal testing machine (TORSEE) with a loading rate of about 0.5 tons per minute. A three points loading was adopted to test the simply supported composite beam specimens. A 75-ton load cell was used to measure the applied load, whereas two linear variable differential transducers (LVDTs) were used to measure the vertical slip between the steel beam and concrete slabs of the pushout test specimens and the mid-span deflection and end slip in the tested composite beam specimens for each load increment, as shown in Figure 5.

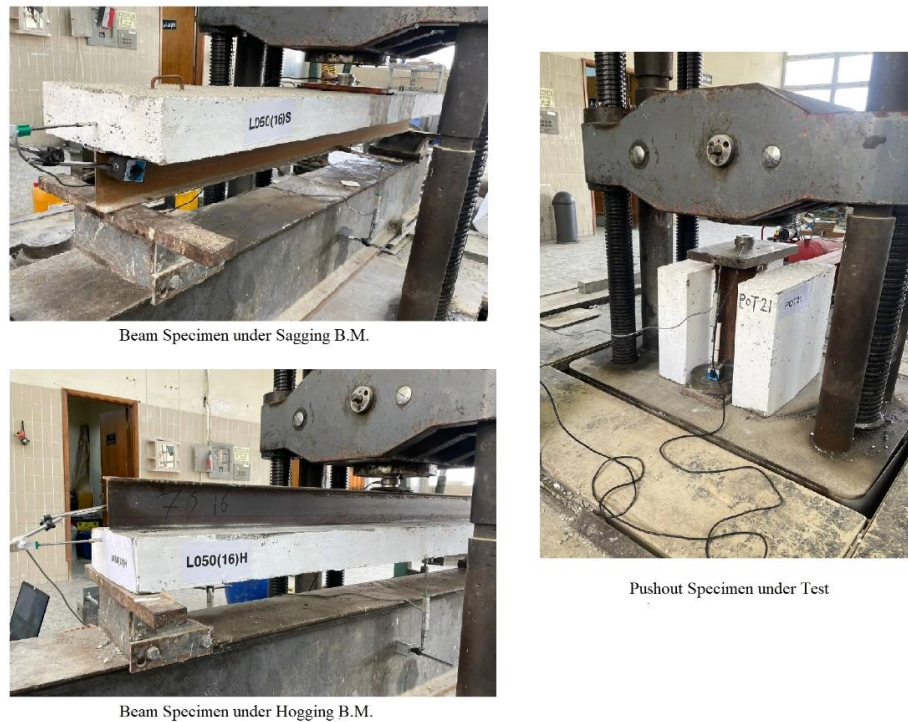


Figure 5. Beam and pushout test specimens under loading

3. Results and Discussion

3.1. Push-Out Tests

3.1.1. Modes of Failure

After the ultimate load was reached, all the pushout test specimens underwent additional loading until one or both slabs detached from the steel beam. It can be seen from Figure 6 that the stud sheared off mode of failure was the main mode of failure in all the tested specimen. It was observed that the headed studs in all cases were failed by shear at the root base. This mode of failure may lead to conclude that the bearing strength of LWSCC at the studs regions and the compressive strength of the specimen's concrete slabs as a whole was greater than the shear strength of the studs. These studs were exhibited to additional stresses during the test, which distributed along the studs' shank which embedded in the LWSCC slabs and concentrated at the root base (at the welding region with the steel section flange) as a weaker point. Table 5 shows the testing findings from the tested pushout specimens.



Figure 6. Failure modes of pushout test specimens

Table 5. Details of findings for the Pushout tested specimens

Specimen's Designation	Stud Ultimate Shear Load (kN)	Ultimate Slip (mm)	Mode of Failure
POT11(16)	71.80	3.11	Stud shear failure
POT12(16)	73.90	2.99	Stud shear failure
POT13(16)	67.50	256	Stud shear failure

3.1.2. Load–Slip Relationships

The mechanical behavior of stud connectors mainly depends on the load-slip curve that developed from the pushout test results. Figure 7 illustrates the load-slip behavior of the tested pushout specimens. It can be observed that the load slip curves for the investigated specimens exhibit a similar pattern that is represented by three different stages. Initially, a linear stage covering about 39% of the ultimate applied load was observed during the test. This stage can be used to evaluate the shear stiffness of the tested pushout specimens, which represents the slope of the load slip curve's linear portion. With approaching to the ultimate load, the second stage can be seen as a nonlinear stage with a significant increase in the vertical slip between the steel section and concrete slabs of the tested specimens. After reaching the specimens' ultimate capacity, the load slip curves showed a third stage, in which the specimens were subjected to further deformation accompanied by a reduction in load until failure occurred. In conclusion, all the test pushout specimens exhibited significant deformation prior to failure, which means that they failed in a ductile mode.

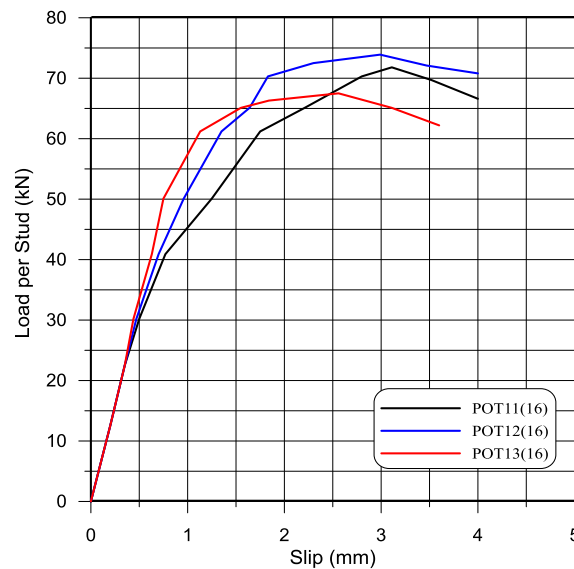


Figure 7. Load–slip curves for the Pushout specimens

3.2. Steel-LWSCC Composite Beams

3.2.1. Failure Modes and Ultimate Strength

When subjected to sagging bending moments, the tested beam specimens exhibited a unique mode of failure (flexural failure) without any sign of failing the connection between the steel beams and concrete slabs. This may lead to the conclusion that the headed stud connection is efficient with the use of LWSCC slabs in composite beams. Accordingly, a composite beam can be constructed efficiently by connecting steel beams to LWSCC slabs using headed stud connections. As expected, the flexural failure mode was initiated by the yielding of steel beams, followed by concrete flange crushing with the increase of the developed compressive stresses at the midspan of the tested beams. As flexural cracks developed in the midspan region of the tested beams, shear flexural cracks also appeared elsewhere. No separation (deponding) emerged between the concrete slab and steel beam in such tested composite beams. Figure 8 demonstrates the modes of failure of the tested steel-LWSCC composite beams under sagging moments, while Table 6 shows that the first visible cracks that appeared in those beams were at a load ranging from 74% to 90% of their ultimate loads.

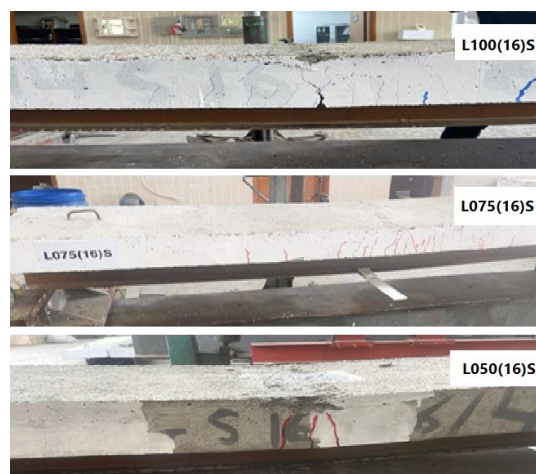


Figure 8. Failure modes and crack patterns for steel-LWSCC beam specimens under sagging bending moment

Table 6. Details of loading stages and modes of failure for composite beam specimens

Specimens' designation	L100(16)S	L075(16)S	L050(16)S	L100(16)H	L075(16)H	L050(16)H	N100(16)S
Ultimate load, P_u (kN)	98.11	79.15	50.43	66.30	52.00	41.56	123.38
First crack load, P_{cr} (kN)	73.00	57.000	45.00	55.00	45.00	40.00	100.00
P_{cr}/P_u (%)	75	72	89	83	86	96	81
Applied bending moment	Sagging	Sagging	Sagging	Hogging	Hogging	Hogging	Sagging
Ultimate Moment Capacity (kN.m)	56.42	45.51	29.00	38.12	30.00	23.92	70.94
Modes of failure	Flexural failure	Flexural failure	Flexural failure	Local buckling	Local buckling shear failure	Longitudinal shear failure	Flexural failure

On the other hand, and as shown in Figure 9, the mode of failure of the tested beam specimens when subjected to the hogging bending moment began with local buckling in the steel beams and was almost followed by a longitudinal shear failure between the concrete slabs and steel beams. This may be related to the movement of the centroid of the composite beam section of the tested specimens toward the concrete slab, producing an increase in the area of the steel section under the effect of compressive stresses. The first visible flexural cracks in such beams appeared at a loading level ranging from 82% to 96% of their failure loads, as listed in Table 6, which was inversely proportional to the degree of shear interaction. The major difference between the modes of failure of these beams and those tested under sagging bending moments is the separation (debonding), which was observed in the tested specimens to have a partial shear interaction between the concrete slab and steel beam.

**Figure 9. Failure modes and crack patterns for steel-LWSCC beam specimens under hogging bending moment**

It was obvious that the ultimate capacity of the tested steel-LWSCC composite beam specimens increased with the increase in DSC, regardless of the nature of the applied bending moment. The effect may be related to the fact that the moment capacity of a composite section depends on the location of the plastic neutral axis within the section. Hence, in the case of a partial shear connection, the compressive force in the concrete slab will decrease with the decrease in DSC due to the reduction in the shear capacity of the headed stud connectors. When comparing the experimental results of steel-LWSCC beam specimens [L050(16)S, L075(16)S, and L100(16)S], which tested under sagging bending moments, and [L050(16)H, L075(16)H, and L100(16)H], which tested under hogging bending moments, It can be observed that the ultimate strength of the specimens tested under the sagging bending moment is increased by a ratio ranging from 18% to 34% compared to those tested under the hogging bending moment at the same DSC because the shear connection is less stiff and has a lower ultimate strength when the concrete slab is in tension.

Relating to Figure 10 and Table 6, the loading level of the crack development at the concrete slabs and their intensity represented the essential differences between the tested beam specimens made of NWSCC and LWSCC. The first visible flexural cracks in beam specimen L100(16)S appeared at a load of about 74% of its ultimate load, while in N100(16)S beam specimen it was about 81% of the ultimate load. The loading level of appearance cracks in the LWSCC slab was earlier than in the NWSCC slab of the tested composite beams, which have the same degree of shear interaction (DSC) and approximately the same concrete compressive strength. Therefore, the steel-NWSCC beam specimen N100(16)S shows less ductility during its loading compared with those that have the same properties but with the lightweight concrete slab L100(16)S.

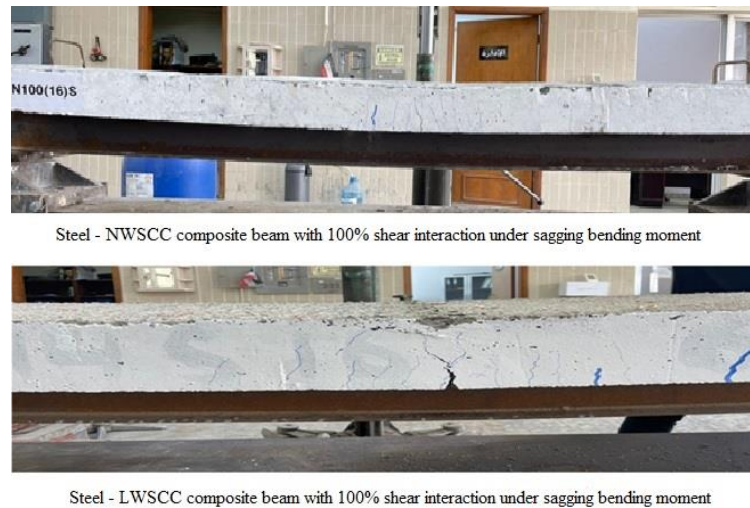


Figure 10. Comparison between modes of failure for NWSCC and LWSCC composite beams

It can be observed from the test results shown in Table 6 that the ultimate strength of the N100(16)S specimen was increased by a ratio of about 21.5% compared to the L100(16)S specimen, which has the same DSC. This may be due to the effect of the relative bond strength of LWSCC, which is always less than the NWSCC due to the replacement of the coarse aggregates with LECA, which has a porous structure.

3.2.2. Load-Deflection Relationships

In general, the midspan deflection of the tested beam specimens increases by an approximate constant small rate with increasing the applied load up to the load level at which the first visible crack appeared. After the appearance of the first visible crack in the concrete slabs of the tested composite beams, the midspan deflection increases at a significant rate until the load reaches the specimen's ultimate capacity. It can be noted from Figures 11 to 13 that the load deflection curves of the tested beams can be divided into two parts: linear and nonlinear. The first part of the curves represents the linear elastic behavior of the tested specimens and covers the region up to the first crack load, while the second part clarifies the tested specimens' nonlinear behavior. When the applied load exceeded the yield load of the tested specimens, a rapid increase in the specimens' deflection was observed, accompanied by a decrease in the load readings until failure.

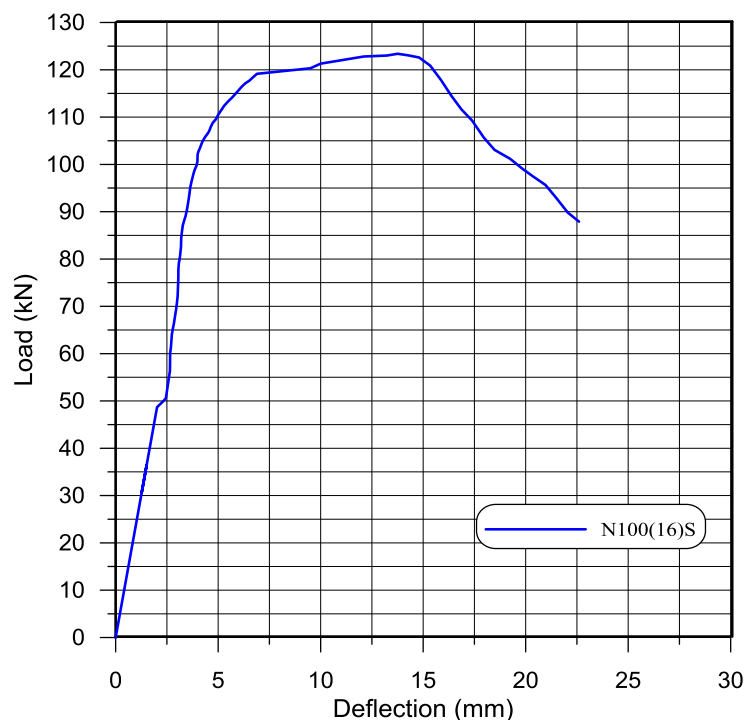


Figure 11. The load-midspan deflection relationship for the steel-NWSCC specimen under sagging bending moment

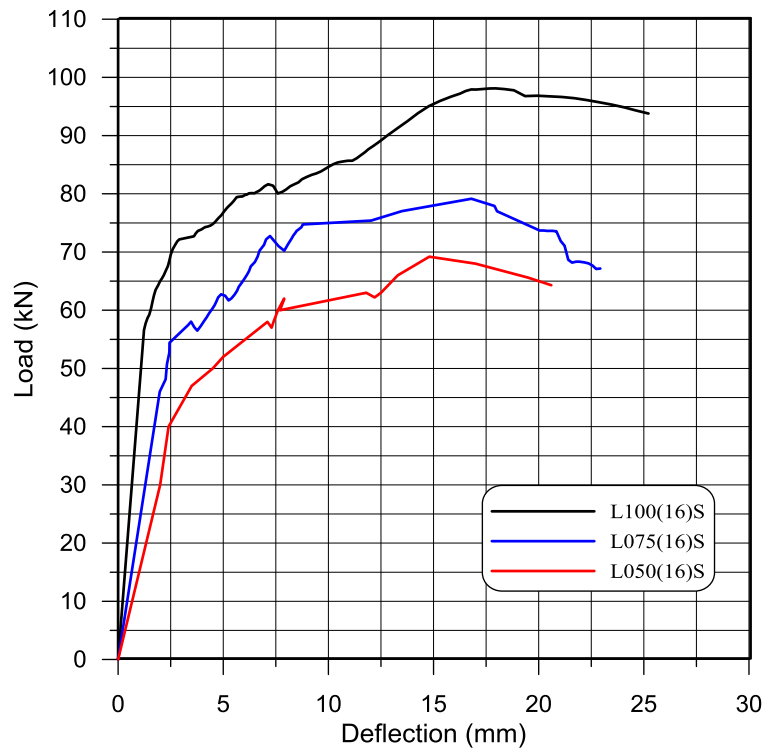


Figure 12. The load-midspan deflection relationship for the steel-LWSCC specimens under sagging bending moment

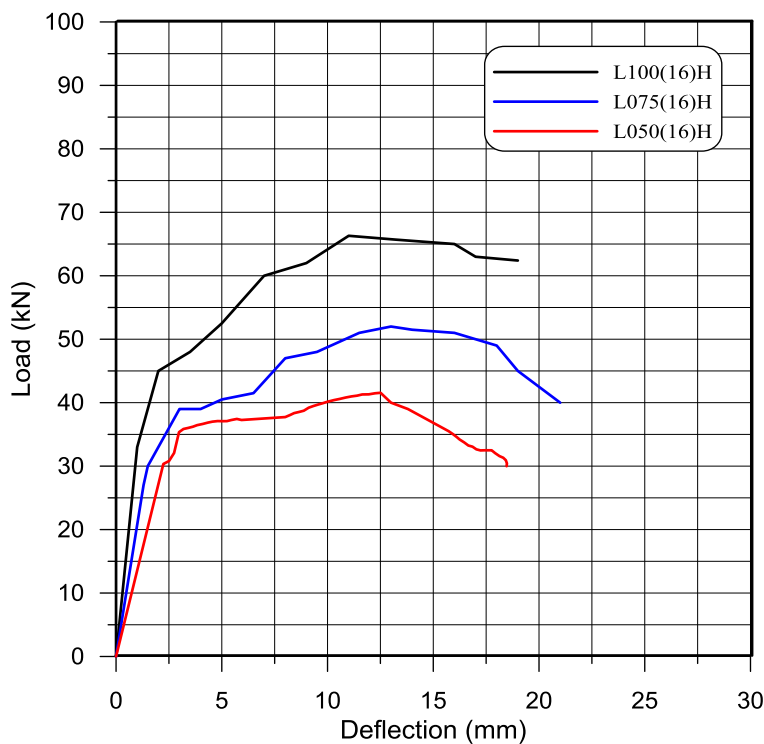


Figure 13. The load-midspan deflection relationship for the steel-LWSCC specimens under hogging bending moment

It can be noted from the results shown in Table 7 that the values of the mid-span deflection at the ultimate load and service load of the steel-LWSCC composite beams [L050(16)S, L075(16)S, and L100(16)S], which tested under the sagging moment, decreased with the increase of DSC due to the increase of the composite beam stiffness. The reason for the increase in stiffness of the composite beam as the DSC increases is related to the fact that the concrete slab and the steel beam of the composite beams behaved and deformed as one unit with the increase in DSC, reducing the relative slip between them, as shown in Figure 14.

Table 7. Experimental results of midspan deflection and stiffness for tested specimens

Specimens' designation	L100(16)S	L075(16)S	L050(16)S	L100(16)H	L075(16)H	L050(16)H	N100(16)S
Ultimate load P_u (kN)	98.11	79.15	50.43	66.30	52.00	41.56	123.38
Deflection at Ultimate Load (mm)	17.95	16.80	14.80	11.00	13.00	12.51	13.76
Service Load (kN)*	65.41	52.77	33.62	44.20	34.67	27.71	82.25
Deflection at Service Load (mm)	2.80	2.50	3.20	1.96	2.20	2.90	3.12
Beam Stiffness (kN/mm)**	23.36	21.11	10.51	22.55	15.76	9.56	26.36

* The service load is two-thirds of the ultimate load

** The beam stiffness is determined by dividing the service load by the corresponding deflection [20].

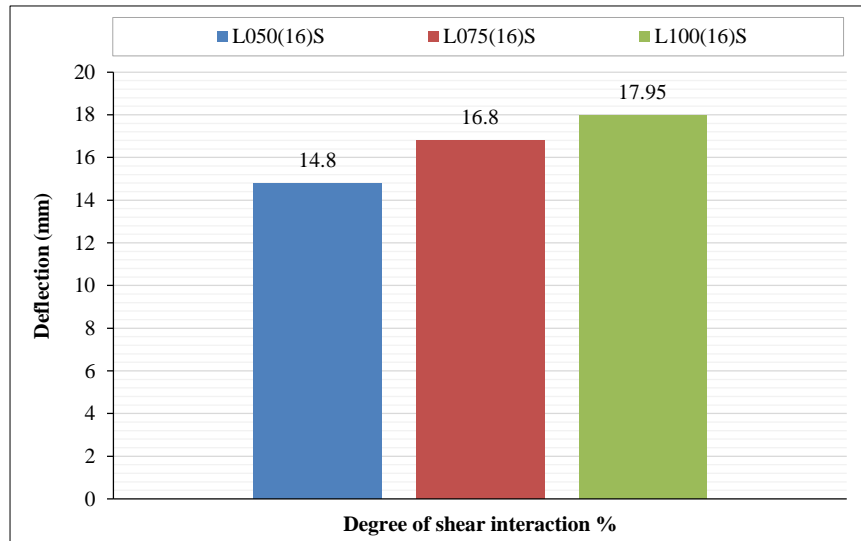


Figure 14. Effect of degree of shear interaction on the deflection of tested composite beam specimens under sagging bending moment

Figure 15 demonstrates the values of deflections for steel-LWSCC beam specimens [L050(16)H, L075(16)H, and L100(16)] that tested under hogging bending moment, which increased by a relatively small amount with the decrease of DSC from 100% to 50%. This is probably related to that, the ultimate capacity of these specimens were convergent and due to the minor role of the concrete slab, which is under tension in such specimens, on the behavior of such composite beams and then less effect for the degree of shear connection. However, the ultimate load and stiffness of these beams are clearly lower than those subjected to sagging bending moment in spite of those beam having the same properties and dimensions as illustrated in Figures 16 to 18. This is clearly related to that the shear connection is less stiff and less ultimate strength when the concrete slab is in tension.

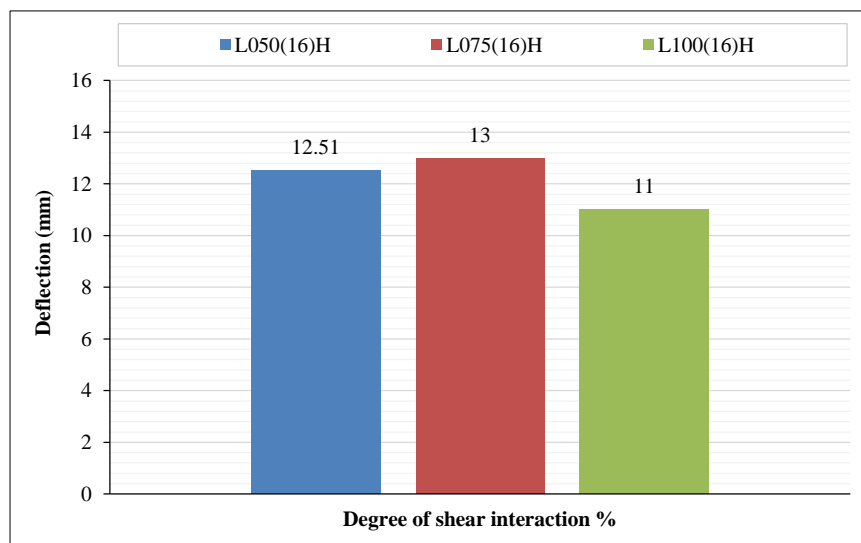


Figure 15. Effect of degree of shear interaction on the deflection of tested composite beam specimens under hogging bending moment

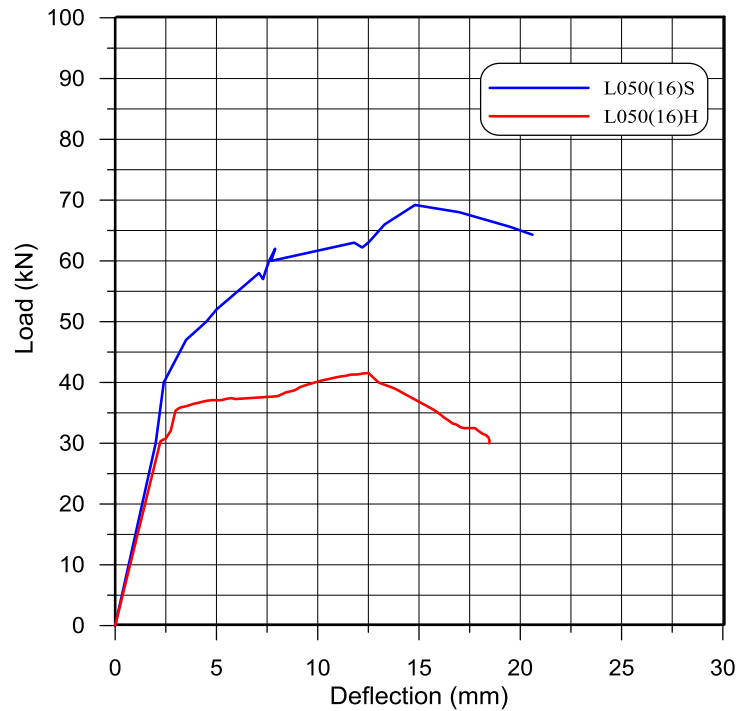


Figure 16. The effect of type of the applied bending moment on the behavior of steel – LWSCC composite beams with 50% degree of shear interaction

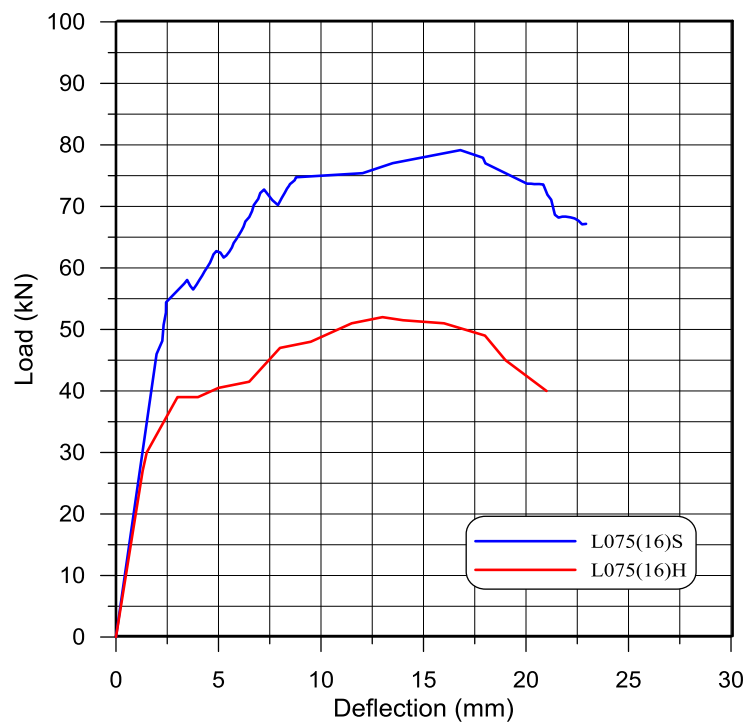


Figure 17. The effect of type of the applied bending moment on the behavior of steel – LWSCC composite beams with 75% degree of shear interaction

3.2.3. Load-Slip Relationships

According to the experimental results of the tested composite beam specimens in the present work with the adopted different degrees of shear interaction and under the effect of sagging or hogging bending moment, an end slip is always existent even with those specimens having full interaction, as illustrated in Table 8. It should be recognized that the stud connectors are flexible, and slip between the concrete slab and the steel beam of the composite beams is inevitable. The load-slip relationships of the tested composite beam specimens in this study are shown in Figures 19 to 21. It can be seen that all the load-slip relationships of the tested beam specimens have the same pattern but differ in their vertex and endpoint positions.

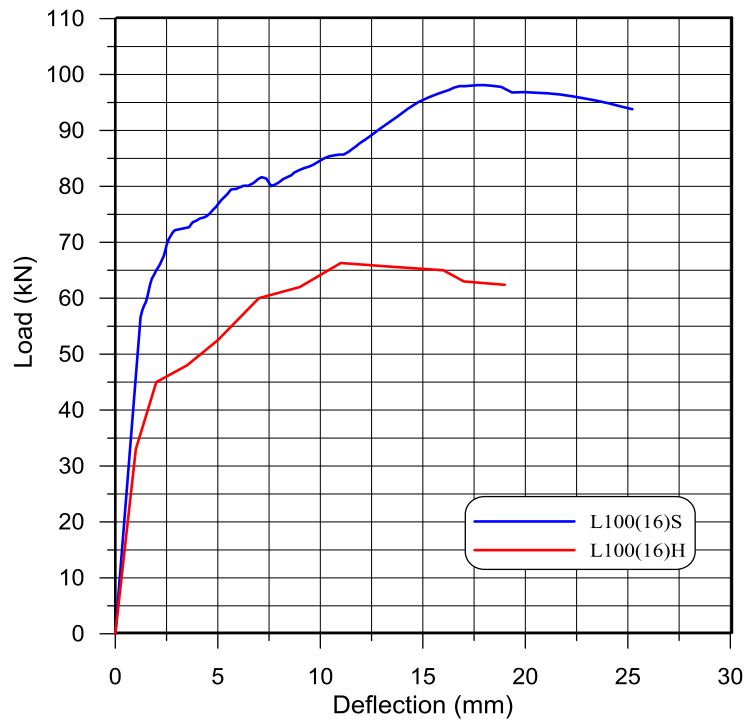


Figure 18. The effect of type of the applied bending moment on the behavior of steel – LWSCC composite beams with 100% degree of interaction

Table 8. The relative end slip corresponding to the ultimate load for all specimens tested

Specimens' designation	L100(16)S	L075(16)S	L050(16)S	L100(16)H	L075(16)H	L050(16)H	N100(16)S
Ultimate loa Pu (kN)	98.11	79.15	50.43	66.30	52.00	41.56	123.38
End Slip at ultimate load(mm)	1.56	3.17	6.10	3.10	4.80	5.60	2.74

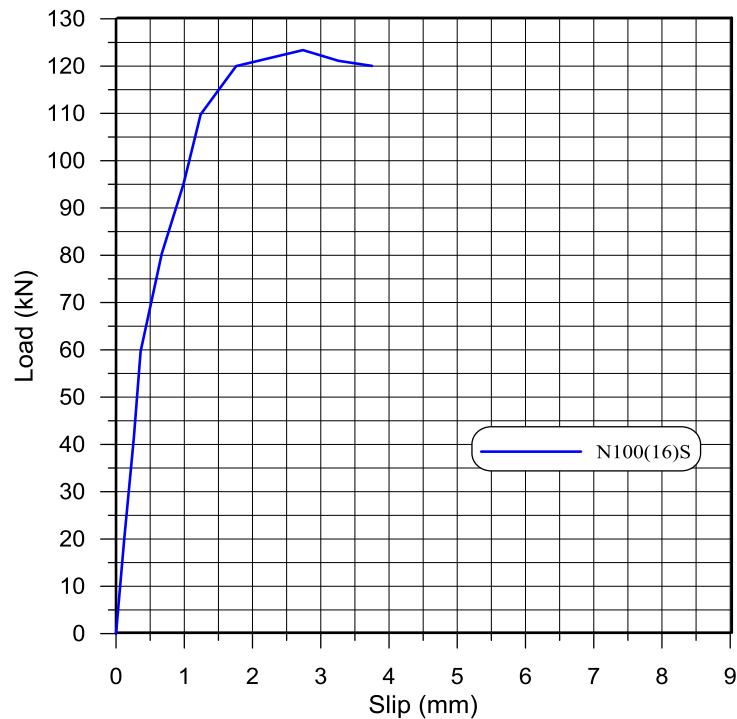


Figure 19. The load-end slip relationship for steel-NWSCC composite beam specimens under sagging bending moment

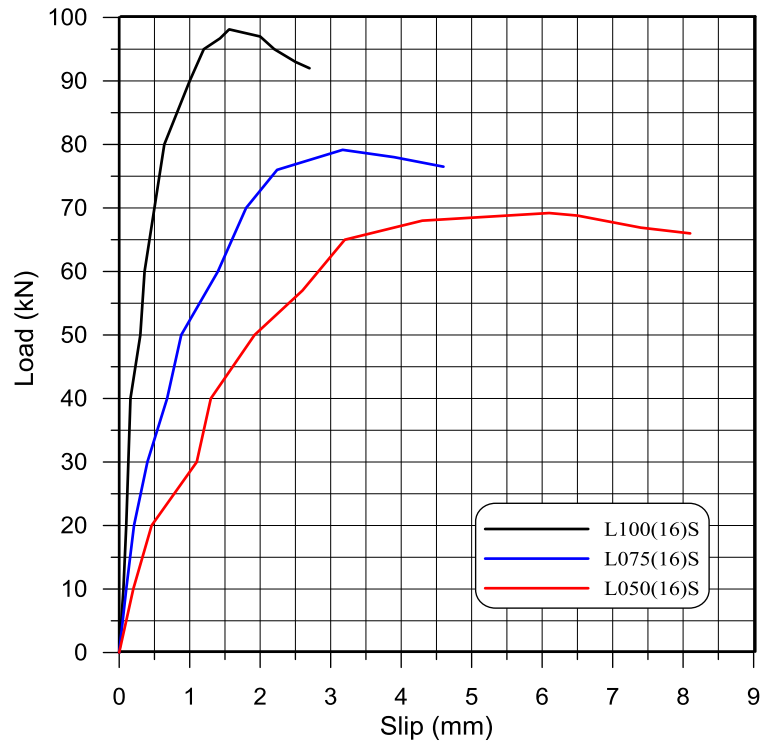


Figure 20. Load – end slip relationship of steel-LWSCC composite beam specimens under sagging bending moment

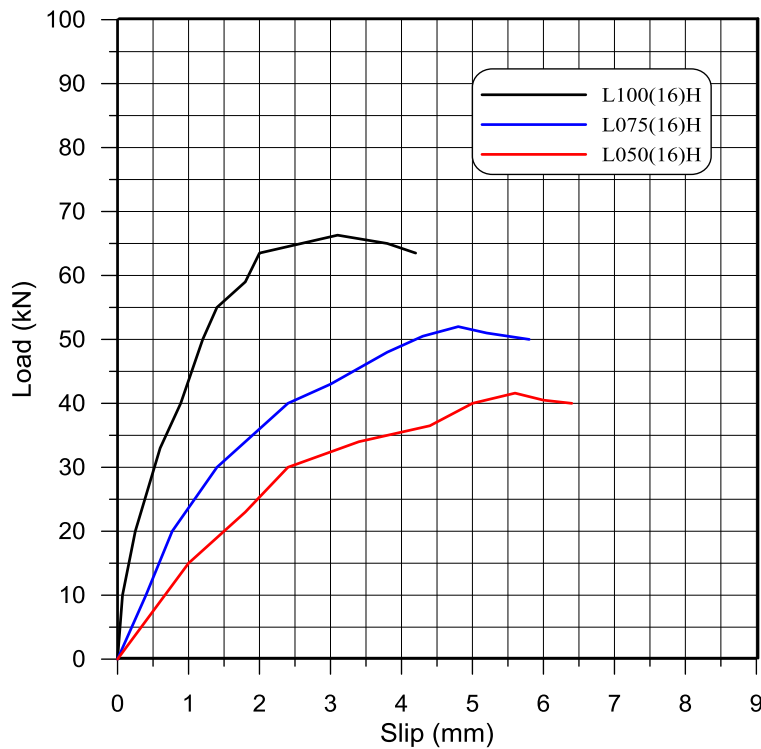


Figure 21. Load – end slip relationship of steel-LWSCC composite beam specimens under hogging bending moment

With the highlight on the relationships between the end slip and the ultimate load for tested beam specimens as listed in Table 8 and shown in Figures 22 and 23, it clearly appeared that the ultimate end slip of the tested specimens is inversely proportional to the degree of shear interaction. This may be related to the increase in shear stiffness of the tested beams with the increase in their degrees of shear interaction.

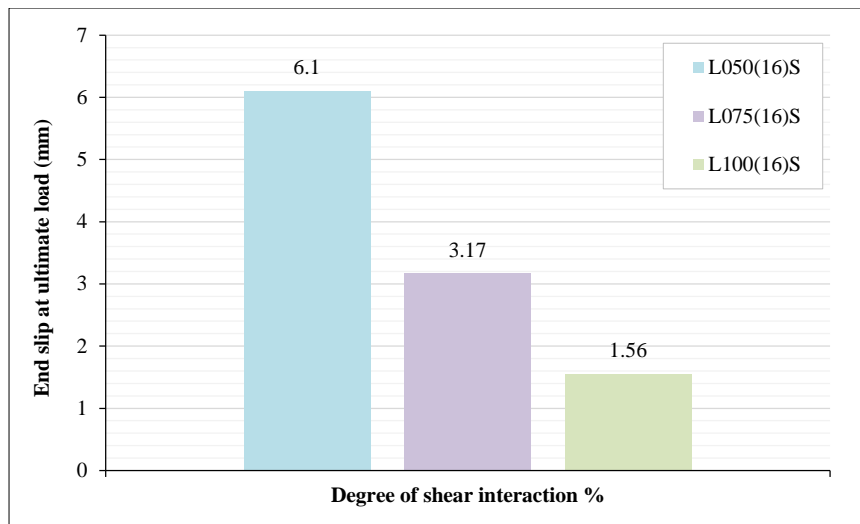


Figure 22. Effect of degree of shear interaction on the end slip of tested composite beam specimens under sagging bending moment

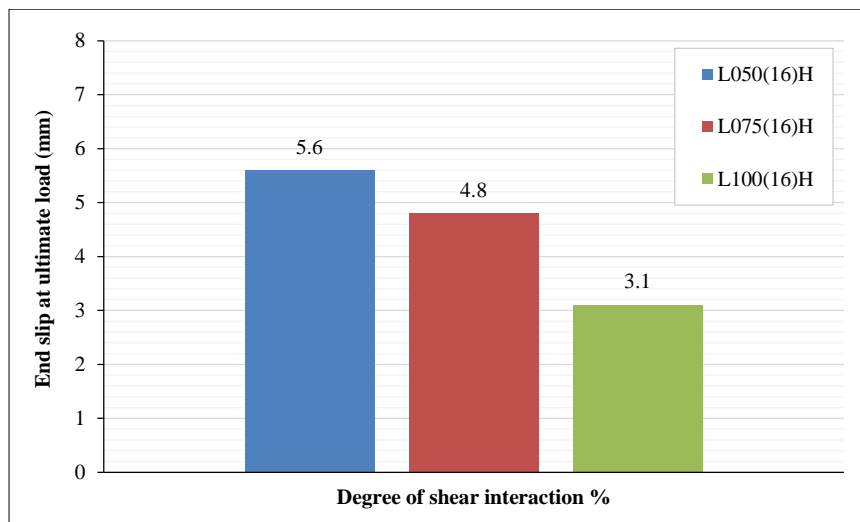


Figure 23. Effect of degree of shear interaction on the end slip of tested composite beam specimens under hogging bending moment

It can be noted that the end slip for the L100(16)S beam specimen was greater than that for the N100(16)S beam specimen at the same load level. Manifesting that the shear connector embedded in LWSCC sustained weaker confinement than in NWSCC due to the replacement of the natural coarse aggregates with LECA. As shown in Table 8, it is obvious that the end slip values for tested specimens under the effect of sagging bending moments were relatively smaller than the values of end slip for the specimens that tested under hogging moments for the same DSC and at the same load level. This is primarily related to the fact that the shear connection is less stiff and has less ultimate strength when the concrete slab of the composite beams is in tension, as previously explained, which leads to an increase in the end slip of the tested beam specimens.

4. Conclusions

The behavior of steel-lightweight self-compacting concrete composite beams was investigated in the present study. Seven beam specimens with different degrees of shear interaction were tested under the effects of sagging and hogging bending moments. Moreover, three pushout test specimens were fabricated and tested in order to evaluate the shear strength of a 16-mm stud diameter when embedded in the lightweight self-compacting concrete. The following points can be concluded from the analysis of the test results:

- In comparison to composite beams with normal-weight slabs, the steel-LWSCC composite beams had only about 11% and 20% less stiffness and ultimate load capacity, respectively, while saving about 24% of their total dead load.
- The maximum deflection for the tested steel-NWSCC composite beams was smaller than that recorded for the tested steel-LWSCC composite beam, which has the same properties but is made of lightweight concrete.

- The stiffness, service load, and ultimate load capacity of the tested steel-LWSCC composite beam specimens were significantly increased with the increase in degree of shear interaction for all the tested beams that tested under sagging or hogging bending moments.
- The ultimate load-carrying capacity of the steel-LWSCC composite beam that tested under hogging bending moments was decreased by a ratio ranging from 17 to 32% at a degree of shear interaction ranging from 50 to 100% compared with steel-LWSCC composite beams that tested under sagging moments.
- In general, the values of the deflection for tested beam specimens at the ultimate load and service load decrease with increasing the degree of shear interaction due to the increase in the composite beams' stiffness.
- The deflection values at the same loads for beams that tested under sagging bending moments are smaller than those for beams that tested under hogging bending moments because the shear connection is less stiff and has less ultimate strength when the concrete slab is in tension.
- When the adopted type of shear connectors in steel concrete composite beams was flexible, like the stud connectors, the relative slip between the concrete slab and the steel beam was inevitable, even if those beams had full interaction.
- The end slip for the tested steel-LWSCC composite beam was larger than that observed in the test of the steel-NWSCC composite beam at the same load level, in spite of the fact that both beams have a full degree of shear interaction.
- The end slip values for tested composite beam specimens under a sagging moment were relatively smaller than the values of end slip for composite beam specimens under hogging moments that have the same degree of shear interaction and at the same load level.

5. Declarations

5.1. Author Contributions

Conceptualization, B.A.H.; methodology, B.A.H.; investigation, B.A.H.; resources, B.A.H. and S.M.S.; data curation, B.A.H.; writing—original draft preparation B.A.H.; writing—review and editing, S.M.S.; supervision, S.M.S.; project administration, S.M.S. All authors have read and agreed to the published version of the manuscript.

5.2. Data Availability Statement

The data presented in this study are available in article.

5.3. Funding

The authors received no financial support for the research, authorship, and/or publication of this article.

5.4. Conflicts of Interest

The authors declare no conflict of interest.

6. References

- [1] Shamass, R., & Cashell, K. A. (2017). Behaviour of Composite Beams Made Using High Strength Steel. *Structures*, 12, 88–101. doi:10.1016/j.istruc.2017.08.005.
- [2] Wang, B., Huang, Q., Liu, X., & Li, W. (2018). Experimental investigation of steel-concrete composite beams with different degrees of shear connection under monotonic and fatigue loads. *Advances in Structural Engineering*, 21(2), 227–240. doi:10.1177/1369433217717121.
- [3] Vasdravellis, G., & Uy, B. (2014). Shear Strength and Moment-Shear Interaction in Steel-Concrete Composite Beams. *Journal of Structural Engineering*, 140(11), 1–11. doi:10.1061/(asce)st.1943-541x.0001008.
- [4] Zhou, M., Zhang, J., Zhong, J., & Zhao, Y. (2016). Shear Stress Calculation and Distribution in Variable Cross Sections of Box Girders with Corrugated Steel Webs. *Journal of Structural Engineering*, 142(6), 1–10. doi:10.1061/(asce)st.1943-541x.0001477.
- [5] Thirumalaiselvi, A., Anandavalli, N., Rajasankar, J., & Iyer, N. R. (2016). Numerical evaluation of deformation capacity of laced steel-concrete composite beams under monotonic loading. *Steel and Composite Structures*, 20(1), 167–184. doi:10.12989/scs.2016.20.1.167.
- [6] Mark Lawson, R., Lam, D., Aggelopoulos, E. S., & Nellinger, S. (2017). Serviceability performance of steel–concrete composite beams. *Proceedings of the Institution of Civil Engineers: Structures and Buildings*, 170(2), 98–114. doi:10.1680/jstbu.16.00048.
- [7] Saleh, S., & Fareed H. AlMosawi, F. H. A. (2018). Behavior of Steel-Normal and High Strength Concrete Composite Beams With Partial Shear Interactionbehavior of Steel-Normal and High Strength Concrete Composite Beams With Partial Shear Interaction. *Kufa Journal of Engineering*, 9(1), 175–190. doi:10.30572/2018/kje/090112.

- [8] Choi, W., Choi, Y., & Yoo, S. W. (2018). Flexural Design and Analysis of Composite Beams with Inverted-T Steel Girder with Ultrahigh Performance Concrete Slab. *Advances in Civil Engineering*, 2018. doi:10.1155/2018/1356027.
- [9] Majeed, F. H. (2018). Behavior of Steel- Lightweight Concrete Composite Beams with Partial Shear Interaction. *Journal of University of Babylon for Engineering Sciences*, 26(2), 20–34. doi:10.29196/jub.v26i2.380.
- [10] Ribeiro Neto, J. G., Vieira, G. S., & Zoccoli, R. de O. (2020). Experimental analysis of the structural behavior of different types of shear connectors in steel-concrete composite beams. *Revista IBRACON de Estruturas e Materiais*, 13(6), 1–17. doi:10.1590/s1983-41952020000600010.
- [11] Zhang, J., Hu, X., Fu, W., Du, H., Sun, Q., & Zhang, Q. (2020). Experimental and theoretical study on longitudinal shear behavior of steel-concrete composite beams. *Journal of Constructional Steel Research*, 171. doi:10.1016/j.jcsr.2020.106144.
- [12] Oliveira, V. M. de, Rossi, A., Ferreira, F. P. V., & Martins, C. H. (2022). Stability behavior of steel–concrete composite cellular beams subjected to hogging moment. *Thin-Walled Structures*, 173, 108987. doi:10.1016/j.tws.2022.108987.
- [13] Yoo, S. W., & Choo, J. F. (2016). Evaluation of the flexural behavior of composite beam with inverted-T steel girder and steel fiber reinforced ultra-high performance concrete slab. *Engineering Structures*, 118, 1-15. doi:10.1016/j.engstruct.2016.03.052.
- [14] Jain, A., Choudhary, R., Gupta, R., & Chaudhary, S. (2020). Abrasion resistance and sorptivity characteristics of SCC containing granite waste. *Materials Today: Proceedings*, 27, 524-528. doi:10.1016/j.matpr.2019.11.318.
- [15] Sadrmomtazi, A., Dolati-Milehsara, S., Lotfi-Omran, O., & Sadeghi-Nik, A. (2016). The combined effects of waste Polyethylene Terephthalate (PET) particles and pozzolanic materials on the properties of self-compacting concrete. *Journal of Cleaner Production*, 112, 2363-2373. doi:10.1016/j.jclepro.2015.09.107.
- [16] Ismail, M. K., & Hassan, A. A. (2022). Performance of lightweight SCC beams strengthened with rubberized engineered cementitious composite in shear. *Engineering Structures*, 252, 113687. doi:10.1016/j.engstruct.2021.113687.
- [17] Uysal, M., & Tanyildizi, H. (2011). Predicting the core compressive strength of self-compacting concrete (SCC) mixtures with mineral additives using artificial neural network. *Construction and Building Materials*, 25(11), 4105-4111. doi:10.1016/j.conbuildmat.2010.11.108.
- [18] Afshoon, I., Miri, M., & Mousavi, S. R. (2023). Comprehensive experimental and numerical modeling of strength parameters of eco-friendly steel fiber reinforced SCC containing coarse copper slag aggregates. *Construction and Building Materials*, 367, 130304. doi:10.1016/j.conbuildmat.2023.130304.
- [19] Li, J., Chen, Y., & Wan, C. (2017). A mix-design method for lightweight aggregate self-compacting concrete based on packing and mortar film thickness theories. *Construction and Building Materials*, 157, 621–634. doi:10.1016/j.conbuildmat.2017.09.141.
- [20] Yu, Z., Tang, R., Cao, P., Huang, Q., Xie, X., & Shi, F. (2019). Multi-axial test and failure criterion analysis on self-compacting lightweight aggregate concrete. *Construction and Building Materials*, 215, 786–798. doi:10.1016/j.conbuildmat.2019.04.236.
- [21] Lv, J., Zhou, T., Du, Q., & Li, K. (2020). Experimental and analytical study on uniaxial compressive fatigue behavior of self-compacting rubber lightweight aggregate concrete. *Construction and Building Materials*, 237, 117623. doi:10.1016/j.conbuildmat.2019.117623.
- [22] Li, J., Zhao, E., Niu, J., & Wan, C. (2021). Study on mixture design method and mechanical properties of steel fiber reinforced self-compacting lightweight aggregate concrete. *Construction and Building Materials*, 267, 121019. doi:10.1016/j.conbuildmat.2020.121019.
- [23] Ting, T. Z. H., Rahman, M. E., Lau, H. H., & Ting, M. Z. Y. (2019). Recent development and perspective of lightweight aggregates based self-compacting concrete. *Construction and Building Materials*, 201, 763–777. doi:10.1016/j.conbuildmat.2018.12.128.
- [24] Lo, T. Y., Tang, P. W. C., Cui, H. Z., & Nadeem, A. (2007). Comparison of workability and mechanical properties of self-compacting lightweight concrete and normal self-compacting concrete. *Materials Research Innovations*, 11(1), 16–17. doi:10.1179/143307507X196239.
- [25] Najim, K. B., & Hall, M. R. (2010). A review of the fresh/hardened properties and applications for plain- (PRC) and self-compacting rubberised concrete (SCRC). *Construction and Building Materials*, 24(11), 2043–2051. doi:10.1016/j.conbuildmat.2010.04.056.
- [26] Gopi, R., Revathi, V., & Kanagaraj, D. (2015). Light expanded clay aggregate and fly ash aggregate as self-curing agents in self-compacting concrete. *Asian Journal of Civil Engineering*, 16(7), 1025–1035.
- [27] Anwar Hossain, K. M. (2004). Properties of volcanic pumice based cement and lightweight concrete. *Cement and Concrete Research*, 34(2), 283–291. doi:10.1016/j.cemconres.2003.08.004.
- [28] Heiza, K., Eid, F., & Masoud, T. (2017). Behavior of Reinforced Concrete Slabs Cast with Light Weight Self Compacting Concrete. *Journal of Engineering Science and Military Technologies*, 17(17), 1–12. doi:10.21608/ejmtc.2017.21604.